

Non-sinusoidal current-phase relation controlled by spin-orbit coupling

Shu-Ichiro Suzuki,¹ Yasuhiro Asano,² and Alexander A. Golubov¹

¹MESA+ Institute for Nanotechnology, University of Twente, 7500 AE Enschede, The Netherlands

²Department of Applied Physics, Hokkaido University, Sapporo 060-8628, Japan

(Dated: April 18, 2023)

We have theoretically shown the origin of the non-sinusoidal current phase relation (CPR). The Josephson current in the ZS/N/ZS junctions changes suddenly its direction at a certain phase difference (i.e., critical phase difference ϕ_c), where ZS and N stand for the Zeeman-splitting superconductor and the normal metal. As a consequence, their CPRs become non-sinusoidal. Calculating the spectral Josephson current, the band-splitting by the Zeeman interaction plays an important role in reversing the current and determines ϕ_c . We have also proposed a method to control non-sinusoidal CPR. The critical phase in the non-sinusoidal CPR can be controlled by tuning the Rashba spin-orbit interaction instead of by manipulating the magnetizations.

I. INTRODUCTION

The Josephson effect is a macroscopic quantum phenomenon.¹ The interference between the electron condensates gives rise to the electric current through the interface. The phase difference between the two pair potentials, which characterise the electron condensates, determines the amount and the direction of the Josephson current. The relation between the current and the phase difference $J(\varphi)$, the so-called current-phase relation (CPR), characterizes Cooper-pair transport mechanisms in Josephson junctions². Analyzing the CPR, for example, one can identify the pairing symmetry of the superconductor, which is essential to reveal the pairing mechanism. With advances in experimental techniques, the CPR recently became a measurable quantity using superconducting quantum interference devices (SQUIDS).^{3–14}

The typical CPR is given by $J \sim \sin \varphi$ which can be realised only in the tunneling limit of the Josephson junction with the BCS-type superconductors or close to T_c of superconducting electrodes. In a more general case in the high-transparency limit, higher harmonics of the CPR are generated. In the ballistic regime, the CPR crosses over to a saw-tooth shape¹⁵ $J \sim \text{sgn}[\varphi/2] \sin(\varphi/2)$ with a jump at $\varphi = \pi$. Recently, it was predicted that 4π -periodic CPR $J \sim \sin(\varphi/2)$ might be realized at low temperatures in a Josephson junction hosting the Majorana bound states (MBSs). The Andreev bound states (ABSs),^{16,17} including the MBSs,^{18–22} stemming from the unconventional Cooper pairing^{23–26} change the transmission of the quasiparticles by the resonant tunneling.^{27–36} The 4π -periodic Josephson current was recently observed in topological superconducting junctions demonstrating the realization of the MBSs.^{7,37,38}

At the same time, the CPR can be qualitatively modified by the Zeeman-splitting (i.e., spin-splitting superconductors^{39–49}). The Josephson current in the diffusive SFcFS junction has been studied using the quasi-classical Usadel theory⁵⁰, where S, F, and c stand for a superconductor, ferromagnetic metal, and constriction,

respectively. It was shown that the Josephson current changes its direction when the phase difference exceeds a certain value ϕ_c (i.e., critical phase difference). In other words, the CPR has an abrupt jump at $\phi = \phi_c$. Such unconventional non-sinusoidal CPR, however, was not detected in experiments yet. To observe this effect, we need to understand how to control this effect to suggest an ideal experimental setting.

In this paper, the one-dimensional Josephson junctions with the Zeeman-splitting superconductors (ZSs) are considered. In particular, we investigate how to maximize the non-sinusoidal behaviour and consider an experimental setup to observe this effect. Using the recursive Green's function (GF) method in the lattice model, we obtain the CPR with varying the junction parameters: magnetizations in the ZSs, junction length, and temperature. We have shown that the non-sinusoidal effect appears when the magnetizations are not antiparallel and can be the most prominent when the magnetizations are parallel. Analyzing the spectral Josephson current, we also show the origin of the non-sinusoidal CPR. We discuss the relation between the critical phase difference and the Andreev level (i.e., the energy level of the quasi-particle bound state at the interface).

In addition, we demonstrate that the non-sinusoidal CPR can be electrically controlled by changing the Rashba spin-orbit coupling (SOC) in the normal segment, which is easier than controlling the magnetizations of the ZSs. The Rashba SOC effectively changes the magne-

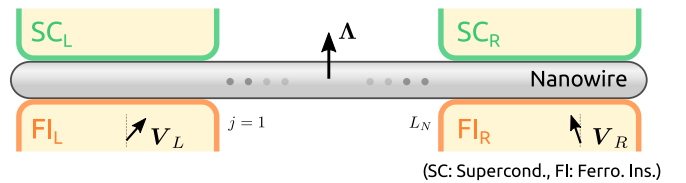


FIG. 1. Schematic of the system. The junction consists of Zeeman-split superconducting regions (ZSs) and a nanowire with a strong spin-orbit interaction. The spin-splitting directions in the SCs are characterised by $V_{L(R)}$. The length of the nanowire is characterized by L_N .

tization configuration of the junction through the spin precession^{51,52} in the normal segment. By changing the Rashba SOC, we can reproduce the whole range of the CPR obtained in the absence of the Rashba SOC.

II. MODEL AND FORMULATION

We consider a one-dimensional Josephson junction with two ZSs. The two ZSs are separated by the normal segment with the length L_N where the Rashba SOC is present. The Zeeman-splitting superconducting state can be realised in the structure show in Fig. 1, where the pair potential and the Zeeman interaction are present in the wire because of the proximity from the conventional superconductors (SCs) and the ferromagnetic insulators.

The Hamiltonian in the normal segment is given by

$$\begin{aligned} \mathcal{H}_N = & -t \sum_{j,\alpha} \left[c_{j+1,\alpha}^\dagger c_{j,\alpha} + c_{j,\alpha}^\dagger c_{j+1,\alpha} \right] \\ & + i \frac{\lambda}{2} \sum_{j,\alpha,\beta} \left[c_{j+1,\alpha}^\dagger (\hat{\sigma}_2)_{\alpha\beta} c_{j,\beta} - c_{j,\alpha}^\dagger (\hat{\sigma}_2)_{\alpha\beta} c_{j+1,\beta} \right] \\ & + \sum_{j,\alpha} c_{j,\alpha}^\dagger (2t - \mu_N) c_{j,\alpha}, \end{aligned} \quad (1)$$

where t , λ , μ_N are the hopping energy, Rashba SOC, chemical potential in the normal segment. The creation and annihilation operators are denoted by $c_{j,\alpha}$ and $c_{j,\alpha}^\dagger$ with the lattice site j and the spin α (β). The Pauli matrices in spin and Nambu space are denoted by σ_ν and τ_ν with $\nu \in \{1, 2, 3\}$, respectively. The identity matrix in each space is defined as σ_0 and τ_0 . In this paper, the accents $\hat{\cdot}$ and $\check{\cdot}$ mean the 2×2 and 4×4 matrices in the spin and Nambu space. The Hamiltonian in the superconducting lead wires are

$$\begin{aligned} \mathcal{H}_i = & -t \sum_{j,\alpha} \left[c_{j+1,\alpha}^\dagger c_{j,\alpha} + c_{j,\alpha}^\dagger c_{j+1,\alpha} \right] \\ & + \sum_{j,\alpha} c_{j,\alpha}^\dagger [(2t - \mu_S) \hat{\sigma}_0 - \mathbf{V}_i \cdot \hat{\boldsymbol{\sigma}}]_{\alpha\beta} c_{j,\beta} \\ & + \sum_j \left[\Delta e^{i\varphi_i} c_{j,\uparrow}^\dagger c_{j,\downarrow}^\dagger + \text{H.c.} \right], \end{aligned} \quad (2)$$

where μ_S is the chemical potential, Δ is the amplitudes of the pair potential, and the subscript $i = L$ (R) specifies the left (right) SC.

The electric current is obtained from the Matsubara GF $\check{\mathcal{G}}_{j,j'}(i\omega_n)$ in the normal segment,^{53–55}

$$J = \frac{ie}{2\hbar} T \sum_{\omega_n} J_n, \quad (3)$$

$$J_n = \text{Tr} \left\{ \check{\tau}_3 [\check{t}_+ \check{\mathcal{G}}_{j,j+1}(i\omega_n) - \check{t}_- \check{\mathcal{G}}_{j+1,j}(i\omega_n)] \right\} \quad (4)$$

with $\omega_n = (2n + 1)\pi T$ is the Matsubara frequency, T is the temperature, and $e < 0$ is the charge of the quasipar-

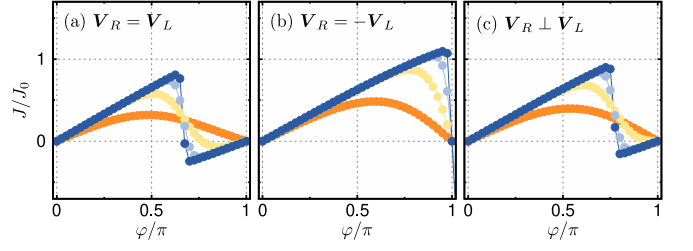


FIG. 2. Current-phase relation in ZS/N/ZS junction. The amplitudes of the magnetization are set to $V_L = V_R = 0.5\Delta_0$. The magnetization in the left is $\mathbf{V}_L \parallel \mathbf{e}_z$ and that in the right is directed to (a) \mathbf{e}_z , (b) $-\mathbf{e}_z$, and (c) \mathbf{e}_y . The temperature is set to $T = T_c 10^{-n_T}$, where n_T varies from -2 (blue line) to -0.5 (orange line) by 0.5 . The length of the junction and the chemical potential are $L_N = 80$ and $\mu_S = \mu_N = 0.5t$.

ticle. The hopping matrix is defined as

$$\check{t}_\pm = \begin{bmatrix} \hat{t}_\pm & 0 \\ 0 & \hat{t}_\pm^* \end{bmatrix}, \quad \hat{t}_\pm = \begin{bmatrix} -t & \mp \lambda/2 \\ \pm \lambda/2 & t \end{bmatrix}. \quad (5)$$

The Josephson current can be calculated also in the real frequency representation with which we can see the relation between the Josephson current and the Andreev levels. The Josephson current is given with the spectral current $J_E(E)$,

$$J = \frac{e}{2\hbar} \int J_E \tanh\left(\frac{E}{2T}\right) dE, \quad (6)$$

$$J_E = \frac{1}{2\pi} \text{Tr} \left\{ \check{\tau}_3 [\check{t}_+ \check{G}_{j,j+1}(E') - \check{t}_- \check{G}_{j+1,j}(E')] \right\}, \quad (7)$$

where $\check{G}_{j,j+1}(E')$ is the retarded GF with $E' = E + i\delta$ with δ being the smearing factor (i.e., an infinitesimal real number).

Throughout this paper, the Matsubara GF $\check{\mathcal{G}}_{j,j'}(i\omega_n)$ and the retarded GF $\check{G}_{j,j'}^R(E)$ are calculated by the recursive GF method⁵⁶. The amplitudes of the magnetization in the ZSs are assumed to be the same ($V = V_L = V_R$ with $V_i = |\mathbf{V}_i|$), whereas the directions can be different. We assume the Zeeman interaction is smaller than $0.5\Delta_0$ so that the pair potentials in the ZSs are finite.^{57,58} The ratio between the zero-temperature pair potential and the hopping energy is set to $\Delta_0 = 0.01t$. The temperature dependence of the pair potential is calculated by the BCS relation. The current density is normalised to $J_0 = |e|\Delta_0/2\hbar$, and the smearing factor is set to $\delta = 0.02\Delta_0$.

III. NON-SINUSOIDAL CURRENT-PHASE RELATION

We first show the numerical results of the CPRs *without* the SOC in Fig. 2. The amplitudes of the magnetizations are set to $V = 0.5\Delta_0$. The magnetizations are (a) parallel, (b) antiparallel, and (c) perpendicular where

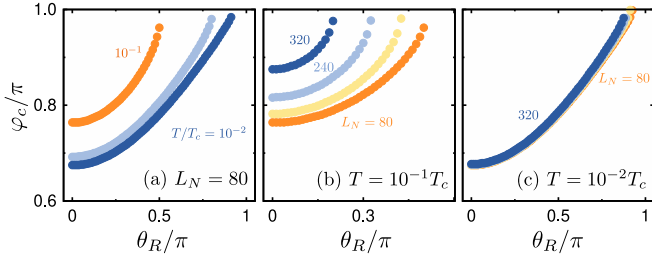


FIG. 3. (a) Temperature dependence of critical phase in ZS/N/ZS junction. The magnetization in the left is $\mathbf{V}_L \parallel \mathbf{e}_z$. The magnetization in the right is $\mathbf{V}_R = \cos\theta_R\mathbf{e}_z + \sin\theta_R\mathbf{e}_x$. The amplitudes of the magnetization are set to $V_L = V_R = 0.5\Delta_0$. The temperature is set to $T = T_c 10^{n_T}$, where n_T varies from -2 to -1 by 0.5 . The length of the junction is $L_N = 80$. (b,c) Length dependence of critical phase. The temperature is set to (b) $T/T_c = 10^{-1}$ and (c) 10^{-2} .

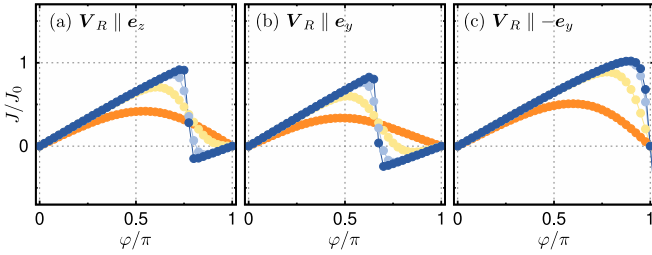


FIG. 4. Current-phase relation in ZS/NW/ZS junction. The spin-orbit coupling in the NW is set to $\lambda = 0.5t$. The magnetization in the left is $\mathbf{V}_L \parallel \mathbf{e}_y$ and that in the right is directed to (a) \mathbf{e}_z , (b) \mathbf{e}_y , and (c) $-\mathbf{e}_y$. The other parameters are set to the same values as used in Fig. 2.

the magnetization in the left SC is fixed to $\mathbf{V}_L \parallel \mathbf{e}_z$. The temperature is set to $T = T_c 10^{n_T}$, where n_T varies from -2 (blue line) to -0.5 (orange line) by 0.5 .

When the magnetizations are parallel [Fig. 2(a)], the Josephson current changes its direction at a certain phase difference at a low temperature. We defined this phase difference as the critical phase difference φ_c . The sign change disappears when the magnetizations are antiparallel [Fig. 2(b)] where the CPR changes from $\sin\phi$ to $\sin(\phi/2)$ as decreasing temperature. The CPRs with parallel and antiparallel configurations are qualitatively the same obtained in the diffusive limit.⁵⁰ In the recursive GF method, we can numerically obtain the CPR with non-collinear magnetizations. When the magnetizations are perpendicular, the abrupt sign change also appears as shown in Fig. 2(c). In this case, the critical phase difference is larger than that in Fig. 2(a).

We show the relations between φ_c and the misalignment of the magnetizations θ_R in Fig. 3, where θ_R is defined as $\mathbf{V}_R = V_L(\cos\theta_R\mathbf{e}_z + \sin\theta_R\mathbf{e}_x)$. Figure 3(a) shows that φ_c minimizes when the magnetizations are parallel ($\theta_R = 0$). The critical phase φ_c approaches π with increasing θ_R , meaning that the non-sinusoidal CPR disappears not only when the magnetizations are antiparallel but also the misalignment is sufficiently larger.

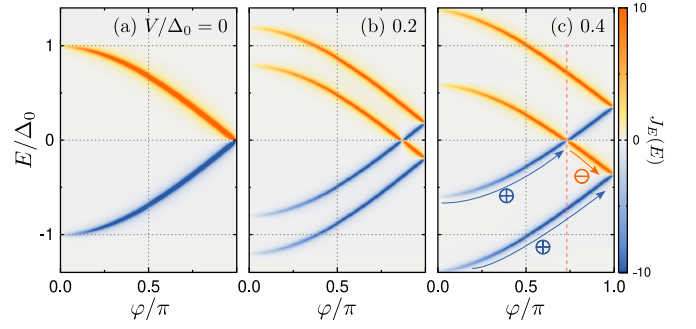


FIG. 5. Spectral Josephson currents in ZS/N/ZS junction *without* spin-orbit coupling. The magnetizations are set to parallel: $\mathbf{V}_R = \mathbf{V}_L = V\mathbf{e}_z$. The amplitude of magnetization is set to (a) $V/\Delta_0 = 0$, (b) 0.2 , and (c) 0.4 . The junction length, the chemical potential, and the smearing factor are set to $L_N = 20$, $\mu = t$, and $\delta = 0.02\Delta_0$. The signs in (c) indicate the sign of the contribution to the total current.

Figure 3(a) also shows that the non-sinusoidal behaviour depends strongly on the temperature. We show the φ_c - θ_R curves for different junction length L_N at $T/T_c = 10^{-1}$ and 10^{-2} in Figs. 3(b) and 3(c) respectively. At the higher temperature [Fig. 3(b)], φ_c becomes larger (i.e., the non-sinusoidal effect becomes weaker) because the thermal smearing diminishes the phase coherence of the quasiparticle. Even when $L_N = 80$, the non-sinusoidal behaviour disappears when $\theta_R \sim 0.5\pi$. In the longer junction, φ_c becomes larger and the non-sinusoidal behaviour disappears with the smaller misalignment θ_R .

At the lower temperature [Fig. 3(c)], the non-sinusoidal behaviour is stable. The critical phase difference φ_c is almost independent of the junction length. At this temperature regime, the coherence length (i.e., $\xi_T \sim \hbar v_F/T$) is much longer than the junction length. In other words, all of the junction in Fig. 3(c) are the short-junction regime (i.e., $\xi_T > L_N$).

The current phase relations *with* the SOC are shown in Fig. 4, where we set $\lambda = 0.5t$. Note that we assume that one of the Zeeman interaction has the same matrix structure as that of the SOC in spin space (i.e., $\mathbf{V}_L \cdot \hat{\sigma} \sim V_L \hat{\sigma}_2 \sim k \hat{\sigma}_2$). The CPRs shown in Fig. 4 are qualitatively the same results as those in Fig. 2 (see Appendix A for details). Namely, the SOC does not play an important role when one of the magnetization is parallel to the SOC in the spin space.

The origin of the non-sinusoidal behaviour can be understood by the spin-band splitting by the Zeeman effects. The spectral Josephson currents $J_E(E)$ [Eq. (7)] are shown in Fig. 5, where we fix (a) $V/\Delta_0 = 0$, (b) 0.2 , and (c) 0.4 with $\mathbf{V}_L \parallel \mathbf{V}_R$, and $L_N = 20$. Note that we need to multiply the factor $\tanh(E/2T)$ to J_E to obtain the total Josephson current. In the absence of the magnetization, the spectral Josephson current has peaks approximately at $E = \pm\Delta_0 \cos(\varphi/2)$ that can be obtained by the Usadel theory in the ZS/constriction/ZC Josephson junction (See Appendix B for details). There are four

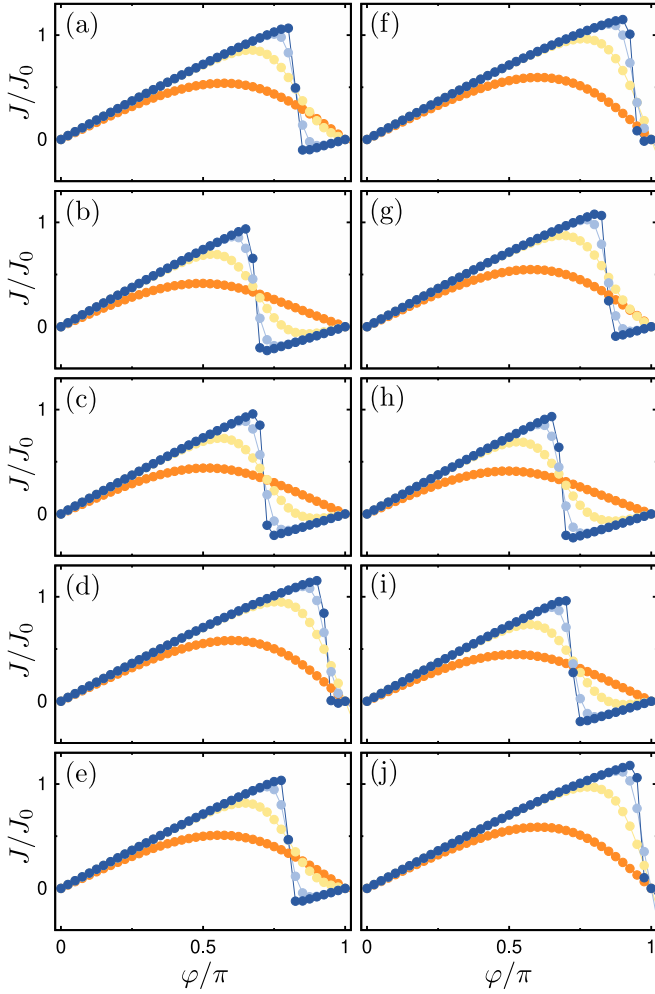


FIG. 6. (a-e) Current phase relation of ZS/NW/ZS junction with the Rashba spin-orbit coupling. The strength of the spin-orbit coupling varies from (a) $\lambda = 0.5t$ to (e) $0.1t$ by $-0.1t$. The critical phase difference depends on λ . The magnetizations are *parallel* $\mathbf{V}_L = \mathbf{V}_R = 0.5\Delta_0 \mathbf{e}_z$. The junction length and the chemical potential are fixed at $L_N = 80$ and $\mu_S = \mu_N = t$. (f-j) Current phase relation with *perpendicular* magnetizations $\mathbf{V}_L = 0.5\Delta_0 \mathbf{e}_z$ and $\mathbf{V}_R = 0.5\Delta_0 \mathbf{e}_x$. These results are plotted in the same manner as in (a-e).

branches in total: two spin-degenerating branches with $J_E > 0$ ($J_E < 0$) in the $E > 0$ ($E < 0$) region.

Under the parallel magnetizations, the Zeeman interaction shifts these branches by $\pm V$ [Fig. 5(b,c)] depending on their spins. When φ is larger than a certain φ_c (i.e., critical phase difference defined from the CPRs), two branches crosses the zero-energy. These branch contributes to the total current in the opposite way to the others because of $\tanh(E/2T)$ [see the indicated signs in Fig. 5(c)]. Therefore, the contributions from the four branches almost cancel each among and the total Josephson current changes suddenly at φ_c .

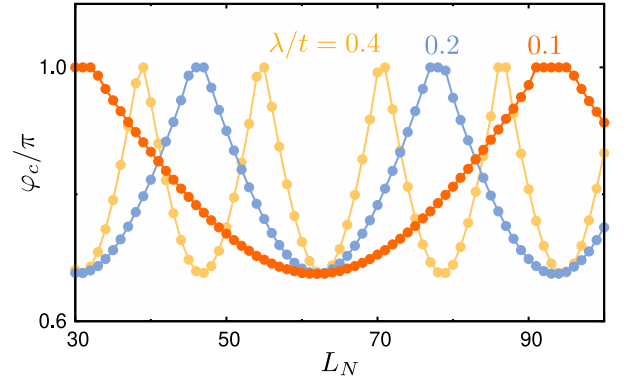


FIG. 7. Junction-length dependences of critical phase difference in ZS/NW/ZS junction. The magnetizations are set to $\mathbf{V}_L = \mathbf{V}_R = 0.5\Delta_0 \mathbf{e}_z$. The spin-orbit coupling is set to $\lambda/t = 0.4, 0.2$, and 0.1 . The temperature is set to $T = 10^{-2}T_c$.

IV. CONTROLLING NON-SINUSOIDAL CURRENT-PHASE RELATIONS

When the Zeeman couplings in both superconductor have a different spin structure from the SOC, the non-sinusoidal effect shows a qualitatively different behavior. The CPRs with $\mathbf{V}_L = \mathbf{V}_R = 0.5\Delta_0 \mathbf{e}_z$ are shown in Fig. 6(a-e) where the SOC varies from (a) $\lambda = 0.5t$ to (e) $0.1t$ by $-0.1t$. As shown in Fig. 6(a-e), the critical phase difference φ_c changes depending on the SOC even at sufficiently low temperature. We also show the results with $\mathbf{V}_R \parallel \mathbf{e}_x$ in Fig. 6(f-j). Although φ_c is different from those in Fig. 6(a-e), φ_c can be controlled by λ as in the parallel configuration. We have confirmed this λ -dependent φ_c never appears when $\mathbf{V}_R \parallel \mathbf{e}_y$ where one of the Zeeman couplings have the same matrix structure as the SOC.

To clarify the relation between φ_c and λ , we show the junction-length dependences of φ_c for several strengths of λ in Fig. 7, where we fix $T = 10^{-2}T_c$ (i.e., short-junction limit). Figure 7 shows φ_c oscillates in the junction length L_N . Even if the magnetization is parallel, non-sinusoidal effect can vanish as happened in the antiparallel configuration [see Fig. 2(b)]. Comparing the results in Fig. 7, we see that the period of oscillation is approximately given by $\sim 1/\lambda$.

The oscillating behaviour is related to the spin precession by the SOC as discussed in Ref. 48. The SOC in the nanowire acts on the quasiparticle spin as an effective Zeeman field and causes the spin precession^{48,51,52}. Corresponding to the SOC, the quasiparticles obtains an additional phase depending on their spin when they travel across the junction. This additional phase can reproduce the situation with the antiparallel magnetizations in the non-SOC junction, where the sudden jump never appears in the CPR [Compare Figs. 6(d) and 2(b)].

The SOC affects on the spectral current as well. The spectral currents are shown in Fig. 8, where $L_N = 80$ and the SOC varies from $\lambda/t = 0.4$ to 0.1 . When

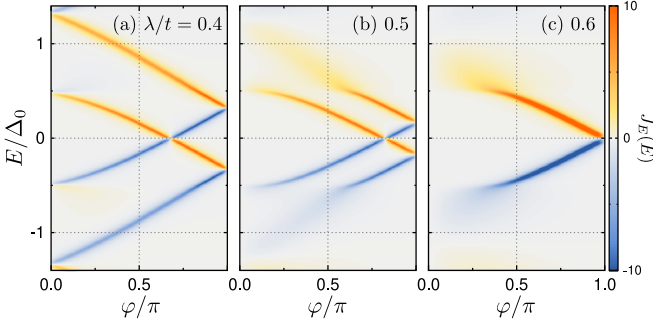


FIG. 8. Junction-length dependence of spectral current in the presence of the spin-orbit coupling. The other parameters are set to the same values in 6(a-e).

$\lambda/t = 0.4$, the band splitting is almost maximized which results in the smallest φ_c [see, for example, Fig. 7]. With increasing the spin-orbit coupling, the band splitting diminishes and becomes almost zero when $\lambda/t = 0.6$. As a consequence, the non-sinusoidal behavior completely disappeared.

The magnitude of the band-splitting in the spectral current is consistent with those obtained in the continuum model.⁴⁸ In the continuous limit, the band splitting is estimated as $\delta E = V \cos(\lambda L_N / \hbar v_F)$, where we have made \hbar explicit to avoid misunderstandings. From this relation, we can estimate the period of the oscillation in Fig. 7 as $L_0 \sim 5.44t/\lambda$ which is consistent with our numerical simulation. In the estimation, the length L_0 is measured in the unit of the lattice constant and we have used $\mu = t$.

V. CONCLUSION

We have shown that the Josephson junction with the Zeeman-splitting superconductors (ZSs) can have a jump in the current-phase relation at the critical phase difference φ_c . In other words, the Josephson current changes suddenly its direction depending on the phase difference. As a result, the current-phase relation (CPR) is no longer sinusoidal. Changing the misalignment between the magnetization in the ZSs, we have shown that ϕ_c depends on the misalignment angle between magnetizations: the non-sinusoidal effect maximises and minimises for the parallel and antiparallel configuration.

Analysing the spectral Josephson current, we have shown that the non-sinusoidal CPR stems from the spin-band splitting by the Zeeman interaction. When the magnetizations are not antiparallel, the level splitting results in the band-splitting in the Andreev levels, resulting in the non-sinusoidal Josephson effect. However, with the antiparallel configuration, the non-sinusoidal behaviour disappears because opposite magnetizations does not split the spin-band of the Andreev levels.

In addition, we have proposed the method to observe the non-sinusoidal CPR. We have demonstrated that the

non-sinusoidal behaviour can be electrically controlled by tuning the Rashba spin-orbit coupling even without changing the magnetizations. The spin-orbit coupling causes the spin precession which controls the width of the spin-band splitting. Namely we can tune the critical phase difference φ_c . In other words, we can switch on and off the non-sinusoidal behaviour without changing the magnetization.

ACKNOWLEDGMENTS

The authors are grateful to Ya. V. Fominov and C. Li for useful discussion. S.-I. S. acknowledges Overseas Research Fellowships by JSPS and the hospitality at the University of Twente. This work was supported by JSPS KAKENHI (No. JP20H01857), JSPS Core-to-Core Program (No. JPJSCCA20170002), and JSPS and Russian Foundation for Basic Research under Japan-Russia Research Cooperative Program (Nos. JPJSBP120194816 and 19-52-50026).

Appendix A: Critical phase difference with spin-orbit coupling

In this section, we discuss ϕ_c in the presence of the Rashba SOC. Note that one of the Zeeman interaction has the same matrix structure as that of the Rashba SOC (i.e., $\mathbf{V}_i \cdot \hat{\boldsymbol{\sigma}} \sim V_i \hat{\sigma}_2 \sim k \hat{\sigma}_2$). The results are shown in Fig. 9 in the same manner as in Fig. 3, where the results without the SOC are shown. Figure 9 shows that, when the one of the Zeeman interaction is proportional to $\hat{\sigma}_y$, the SOC with $k_x \hat{\sigma}_y$ does not qualitatively change ϕ_c .

Appendix B: Gor'kov theory and non-sinusoidal current-phase relation

1. Usadel theory

In a diffusive superconducting system in equilibrium, the Usadel quasiclassical Green's functions satisfy the Usadel equation:

$$\hbar D \nabla \cdot (\check{g} \nabla \check{g}) + i [\omega_n \check{\tau}_3 + \check{H}, \check{g}]_- = 0, \quad (\text{B1})$$

where D is the diffusion constant and $\check{g} = \check{g}(\mathbf{r}, i\omega_n)$ is the Matsubara Green's function in the Nambu space (i.e., particle-hole \otimes spin space) defined as,

$$\check{g} = \begin{pmatrix} \hat{g} & \hat{f}_\omega \\ \hat{f}_{-\omega}^\dagger & -\hat{g} \end{pmatrix}. \quad (\text{B2})$$

In Eq. (B2), we have used the symmetry of the Green's function: $-\hat{f}_\omega = \hat{f}_{-\omega}^\dagger$ with the undertilde functions de-

defined as $\hat{X}(\mathbf{r}, i\omega_n) = \hat{X}(\mathbf{r}, i\omega_n)^*$ with X being an arbitral function.

In this note, we assume the Zeeman and the s -wave spin-singlet pair potentials. The \tilde{H} -matrix in this case is given by

$$\tilde{H} = \begin{bmatrix} \hat{\xi} & \hat{\eta} \\ \hat{\eta}^\dagger & \hat{\xi} \end{bmatrix} = \begin{bmatrix} -V\hat{\sigma}_3 & i\Delta_0(i\hat{\sigma}_2) \\ i\Delta_0^*(i\hat{\sigma}_2)^\dagger & -V\hat{\sigma}_3 \end{bmatrix}, \quad (\text{B3})$$

where we have assumed the Zeeman potential $V(x)$ is in the σ_3 -direction. In this case, it is convenient to apply the unitary transform,

$$\tilde{U}^{-1}(i\omega_n\tilde{\tau}_3 + \tilde{H})\tilde{U} \quad (\text{B4})$$

$$= \begin{bmatrix} i\omega_n - V\hat{\sigma}_3 & i\Delta_0\hat{\sigma}_0 \\ i\Delta_0^*\hat{\sigma}_0 & -i\omega_n + V\hat{\sigma}_3 \end{bmatrix}, \quad (\text{B5})$$

with $\tilde{U} = \text{diag}[\hat{\sigma}_0, -i\hat{\sigma}_2]$. Accordingly, the Green's function can be parametrised as,

$$\tilde{U}^{-1}\tilde{g}\tilde{U} = \begin{pmatrix} g_+ & 0 & f_{\omega,+} & 0 \\ 0 & g_- & 0 & f_{\omega,-} \\ f_{-\omega,+}^* & 0 & -g_- & 0 \\ 0 & f_{-\omega,-}^* & 0 & -g_+ \end{pmatrix}. \quad (\text{B6})$$

where we have used $\hat{g} = \text{diag}[g_+, g_-]$ and $\hat{f}_\omega = \text{diag}[f_{\omega,+}, f_{\omega,-}](i\hat{\sigma}_2)$. Therefore, in the following, we treat this spin-reduced Green's function in each spin subspace,

$$\tilde{g}_\sigma = \begin{pmatrix} g_\sigma & f_{\omega,\sigma} \\ f_{-\omega,\sigma}^* & -g_{\bar{\sigma}} \end{pmatrix} = \begin{pmatrix} g_\sigma & f_{\omega,\sigma} \\ \underline{f}_{\omega,\sigma} & -\underline{g}_{\bar{\sigma}} \end{pmatrix}, \quad (\text{B7})$$

where $\sigma = \pm$ (with $\bar{\sigma} = -\sigma$) specifies the spin subspace. We have introduced the underline accent as $\underline{f}_\omega = f_{-\omega}^*$. The normalization condition becomes

$$g_\sigma^2 + f_\sigma \underline{f}_\sigma = 1. \quad (\text{B8})$$

In the homogeneous limit, the Green's functions satisfy

$$\tilde{g}_\sigma = \frac{1}{\Omega_\sigma} \begin{bmatrix} \omega_\sigma & \Delta_0 \\ \Delta_0^* & -\omega_\sigma \end{bmatrix}, \quad (\text{B9})$$

with $\Omega_\sigma = \sqrt{\omega_\sigma^2 + |\Delta_0|^2}$ and $\omega_\sigma = \omega_n + i\sigma V$.

2. Josephson current

In this section, we consider the superconductor/constriction/superconductor junction as discussed, for example, in Ref. 50. The Josephson current in an

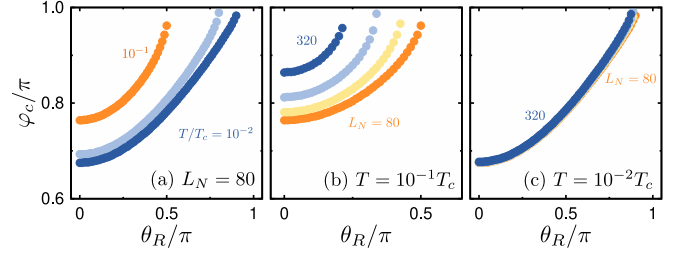


FIG. 9. (a) Temperature dependence of critical phase in ZS/NW/ZS junction. (b,c) Length dependence of critical phase. The magnetization in the left is $\mathbf{V}_L \parallel \mathbf{e}_y$. The magnetization in the right is $\mathbf{V}_R = \cos \theta_R \mathbf{e}_y + \sin \theta_R \mathbf{e}_z$. The results are shown in the same manner as in Fig. 3.

ScS junction can be written as,

$$J = \frac{\pi T}{2i|e|R_N} \sum_{\omega_n, \sigma} J_\sigma(i\omega_n), \quad (\text{B10})$$

$$J_\sigma = \frac{(\underline{f}_{L,\sigma} f_{R,\sigma} - f_{L,\sigma} \underline{f}_{R,\sigma})/2}{2 - D[1 - g_{L,\sigma} g_{R,\sigma} - (\underline{f}_{L,\sigma} f_{R,\sigma} + f_{L,\sigma} \underline{f}_{R,\sigma})/2]}. \quad (\text{B11})$$

where the subscript $i = L (R)$ specifies the left (right) superconductor.⁶¹

Assuming the Zeeman-splitting superconductors, the Green's functions are given by

$$g_{i,\sigma} = \omega_{i,\sigma}/\Omega_{i,\sigma}, \quad f_{i,\sigma} = \Delta e^{i\varphi_i}/\Omega_{i,\sigma}, \quad (\text{B12})$$

where $\omega_{i,\sigma} = \omega_n + i\sigma V_i$, $\Omega_{i,\sigma} = \sqrt{\omega_{i,\sigma}^2 - \Delta_0^2}$. The current across the junction can be obtained as

$$I = \frac{\pi T}{i|e|R_N} \sum_{\omega_n, \sigma} J_\sigma(i\omega_n), \quad (\text{B13})$$

$$J_\sigma(i\omega_n) = \frac{i\Delta_0^2 \sin \varphi}{2\Omega_L \Omega_R - D[\Omega_L \Omega_R - \omega_L \omega_R - \Delta_0^2 \cos \varphi]}. \quad (\text{B14})$$

where we have omitted σ . When the magnetizations are parallel ($V_L = V_R$), the current density is reduced to

$$I = \frac{2\pi T}{|e|R_N} \sum_{\omega_n > 0} \frac{A\Delta_0^2 \sin \varphi}{A^2 + 4\omega_n^2 V^2}, \quad (\text{B15})$$

$$A = (\omega_n^2 - V^2) + \Delta_0^2[1 - D \sin^2(\varphi/2)]. \quad (\text{B16})$$

In this expression, the factor A has a sign change at

$$\sin^2(\varphi_c/2) = \frac{\Delta_0^2 - V^2 + \omega_n^2}{D\Delta_0^2} \quad (\text{B17})$$

meaning that the Josephson current suddenly changes the direction at a certain phase difference φ_c (i.e., non-sinusoidal effect). In the antiparallel junction ($V_L = -V_R$), the CPR is a standard one (i.e., no jump appears

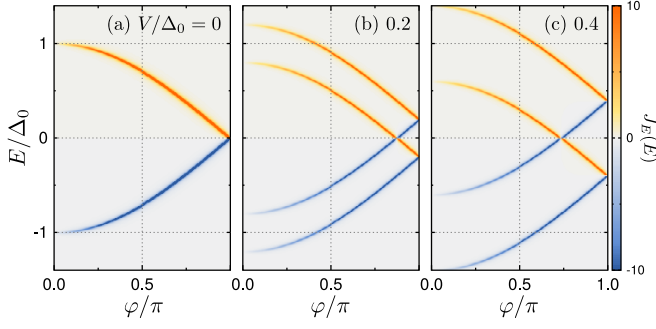


FIG. 10. Spectral Josephson current in ScS junction obtained by the Usadel theory.

in the CPR) because the extra phases from the Zeeman effects cancel each other; $\omega_R = \omega_L^*$ and $\Omega_R = \Omega_L^*$.

Using the analytic continuation, we can obtain the expression of the current in the real-frequency representation. When the magnetizations are parallel, the current in terms of the spectral current is given by

$$J = \frac{\pi}{|e|R_N} \int J_E \tanh\left(\frac{E}{2T}\right) dE, \quad (\text{B18})$$

$$J_E = -\frac{1}{2\pi}(J^R - J^A), \quad (\text{B19})$$

$$J^R = \sum_{\sigma} \frac{i\Delta_0^2 \sin \varphi}{\Delta_0^2 [1 - D \sin^2(\varphi/2)] - (\bar{E}^2 - V^2)}. \quad (\text{B20})$$

where $\bar{E} = E + i\delta$. Using the relation $J^A = -(J^R)^*$, we have

$$J_E = \sum_{\sigma} J_{E,\sigma}, \quad (\text{B21})$$

$$J_{E,\sigma} = \frac{1}{2\pi} \frac{\Delta_0^2 \sin \varphi \delta_1}{\Delta_1^2 + \delta_1^2}, \quad (\text{B22})$$

$$\Delta_1 = \Delta_0^2 [1 - D \sin^2(\varphi/2)] - (E - \sigma V)^2, \quad (\text{B23})$$

where $\delta_1 = 2(E - V)\delta$. Equation (B22) become the Lorentzian-type Dirac function at $\delta_1 \rightarrow 0$ that has peaks at

$$E = \pm \sqrt{1 - D \sin^2(\phi/2)} + \sigma V, \quad (\text{B24})$$

which can reproduce the results in the high-transparency limit in the absence and presence of the Zeeman field.^{48,62} The peak positions are shifted by the Zeeman interaction in the superconductors. The spectral currents J_E are shown in Fig. 10, where (a) $V/\Delta_0 = 0$, (b) 0.2, and (c) 0.4. The results are qualitatively the same as those in Fig. 5.

-
- ¹ B. Josephson, *Phys. Lett.* **1**, 251 (1962).
 - ² A.A. Golubov, M.Yu. Kupriyanov, E. Il'ichev, *Rev. Mod. Phys.* **76**, 411 (2004).
 - ³ M. L. Della Rocca, M. Chauvin, B. Huard, H. Pothier, D. Esteve, and C. Urbina, *Phys. Rev. Lett.* **99**, 127005 (2007).
 - ⁴ G.-H. Lee, S. Kim, S.-H. Jhi, and H.-J. Lee, *Nat. Commun.* **6**, 6181 (2015).
 - ⁵ G. Nanda, J. L. Aguilera-Servin, P. Rakytá, A. Kormányos, R. Kleiner, D. Koelle, K. Watanabe, T. Taniguchi, L. M. K. Vandersypen, and S. Goswami, *Nano Lett.* **17**, 3396 (2017).
 - ⁶ A. Murani, A. Kasumov, S. Sengupta, Yu. A. Kasumov, V. T. Volkov, I. I. Khodos, F. Brisset, R. Delagrange, A. Chepelianskii, R. Deblock, H. Bouchiat, and S. Guéron, *Nat. Commun.* **8**, 15941 (2017).
 - ⁷ C. Li, J. C. de Boer, B. de Ronde, S. V. Ramankutty, E. van Heumen, Y. Huang, A. de Visser, A. A. Golubov, M. S. Golden, and A. Brinkman, *Nat. Mater.* **17**, 875 (2018).
 - ⁸ L. V. Ginzburg, I. E. Batov, V. V. Bol'ginov, S. V. Egorov, V. I. Chichkov, A. E. Shchegolev, N. V. Klenov, I. I. Soloviev, S. V. Bakurskiy, and M. Yu. Kupriyanov *JETP Lett.* **107**, 48 (2018).
 - ⁹ M. Kayyalha, M. Kargarian, A. Kazakov, I. Miotkowski, V. M. Galitski, V. M. Yakovenko, L. P. Rokhinson, and Y. P. Chen, *Phys. Rev. Lett.* **122**, 047003 (2019).
 - ¹⁰ F. Nichele, E. Portolès, A. Fornieri, A. M. Whitticar, A. C. C. Drachmann, S. Gronin, T. Wang, G. C. Gardner, C. Thomas, A. T. Hatke, M. J. Manfra, and C. M. Marcus, *Phys. Rev. Lett.* **124**, 226801 (2020).
 - ¹¹ M. Kayyalha, A. Kazakov, I. Miotkowski, S. Khlebnikov, L. P. Rokhinson, and Y. P. Chen, *npj Quantum Materials* **5**, 7 (2020).
 - ¹² Ya. V. Fominov and D. S. Mikhailov, *Phys. Rev. B* **106**, 134514 (2022).
 - ¹³ M. Endres, A. Kononov, H. S. Arachchige, J. Yan, D. Mandrus, K. Watanabe, T. Taniguchi, C. Schönenberger, *arXiv:2211.10273* (2022).
 - ¹⁴ I. Babich, A. Kudriashov, D. Baranov, V. Stolyarov, *arXiv:2302.02705* (2023).
 - ¹⁵ I.O. Kulik and A. N. Omelyanchuk, *JETP Lett.* **21**, 96 (1975).
 - ¹⁶ J. Hara and K. Nagai, A Polar State in a Slab as a Soluble Model of p-Wave Fermi Superfluid in Finite Geometry *Prog. Theor. Phys.* **76**, 1237 (1986).
 - ¹⁷ C.-R. Hu, *Phys. Rev. Lett.* **72**, 1526 (1994).
 - ¹⁸ M. Sato, Y. Takahashi, and S. Fujimoto, *Phys. Rev. Lett.* **103**, 020401 (2009).
 - ¹⁹ R. M. Lutchyn, J. D. Sau, and S. Das Sarma, *Phys. Rev. Lett.* **105**, 077001 (2010).
 - ²⁰ Y. Oreg, G. Refael, and F. von Oppen, *Phys. Rev. Lett.* **105**, 177002 (2010).
 - ²¹ R. S. Akzyanov, A. L. Rakhmanov, A. V. Rozhkov, and F. Nori, *Phys. Rev. B* **94**, 125428 (2016).
 - ²² S.-I. Suzuki, Y. Kawaguchi, and Y. Tanaka, *Phys. Rev. B* **97**, 144516 (2018).
 - ²³ S.-I. Suzuki and Y. Asano, *Phys. Rev. B* **89**, 184508 (2014);

- 91**, 214510 (2015); **94**, 155302 (2016).
- ²⁴ S.-I. Suzuki, T. Hirai, M. Eschrig, and Y. Tanaka, *Phys. Rev. Res.* **3**, 043148 (2021).
 - ²⁵ S.-I. Suzuki, S. Ikegaya, A. A. Golubov, *Phys. Rev. Res.* **4**, L042020 (2022).
 - ²⁶ S. Yoshida, S.-I. Suzuki, and Y. Tanaka, *Phys. Rev. Res.* **4**, 043122 (2022).
 - ²⁷ Y. Tanaka and S. Kashiwaya, *Phys. Rev. Lett.* **74**, 3451 (1995).
 - ²⁸ S. Kashiwaya and Y. Tanaka, *Rep. Prog. Phys.* **63**, 1641 (2000).
 - ²⁹ Y. Asano, Y. Tanaka, and S. Kashiwaya, *Phys. Rev. B* **69**, 134501 (2004).
 - ³⁰ D. Daghero, M. Tortello, G. Ummarino *et al.*, *Nat. Commun.* **3**, 786 (2012).
 - ³¹ S. Ikegaya, S.-I. Suzuki, Y. Tanaka, and Y. Asano, *Phys. Rev. B* **94**, 054512 (2016).
 - ³² L. Aggarwal, A. Gaurav, G. Thakur *et al.*, *Nat. Mater.* **15**, 32 (2016).
 - ³³ L. A. B. Olde Olthof, S.-I. Suzuki, A. A. Golubov, M. Kunieda, S. Yonezawa, Y. Maeno, and Y. Tanaka, *Phys. Rev. B* **98**, 014508 (2018).
 - ³⁴ S.-I. Suzuki, M. Sato, and Y. Tanaka, *Phys. Rev. B* **101**, 054505 (2020).
 - ³⁵ Y. Takabatake, S.-I. Suzuki, and Y. Tanaka, *Phys. Rev. B* **103**, 184515 (2021).
 - ³⁶ S. Ikegaya, S.-I. Suzuki, Y. Tanaka, and D. Manske, *Phys. Rev. Res.* **3**, L032062 (2021).
 - ³⁷ J. Wiedenmann, E. Bocquillon, R. S. Deacon, S. Hartinger, O. Herrmann, T. M. Klapwijk, L. Maier, C. Ames, C. Brüne, C. Gould, A. Oiwa, K. Ishibashi, S. Tarucha, H. Buhmann, and L. W. Molenkamp, *Nat. Commun.* **7**, 10303 (2016).
 - ³⁸ A.-Q. Wang, C.-Z. Li, C. Li, Z.-M. Liao, A. Brinkman, and D.-P. Yu, *Phys. Rev. Lett.* **121**, 237701 (2018).
 - ³⁹ R. Meservey, P. M. Tedrow, and Peter Fulde, *Phys. Rev. Lett.* **25**, 1270 (1970).
 - ⁴⁰ R. Meservey and P. Tedrow, *Phys. Rep.* **238**, 173 (1994).
 - ⁴¹ F. S. Bergeret, A. F. Volkov, and K. B. Efetov, *Phys. Rev. Lett.* **86**, 3140 (2001).
 - ⁴² X. Li, Z. Zheng, D. Y. Xing, G. Sun, and Z. Dong, *Phys. Rev. B* **65**, 134507 (2002).
 - ⁴³ F. Giazotto and F. Taddei, *Phys. Rev. B* **77**, 132501 (2008).
 - ⁴⁴ T. Yokoyama, M. Eto, and Y. V. Nazarov, *Phys. Rev. B* **89**, 195407 (2014).
 - ⁴⁵ H. Emamipour, *Chin. Phys. B* **23**, 057402 (2014).
 - ⁴⁶ M. Eschrig, *Rep. Prog. Phys.* **78**, 104501 (2015).
 - ⁴⁷ J. Linder and J. W. A. Robinson, *Nat. Phys.* **11**, 307 (2015).
 - ⁴⁸ T. Hashimoto, A. A. Golubov, Y. Tanaka, and J. Linder, *Phys. Rev. B* **96**, 134508 (2017).
 - ⁴⁹ A. Maiani, K. Flensberg, M. Leijnse, C. Schrade, S. Vaitiekėnas, R. S. Souto, *arXiv:2302.04267* (2023).
 - ⁵⁰ A. A. Golubov, M. Yu. Kupriyanov, and Ya. V. Fominov, *JETP Lett.* **75**, 588 (2002).
 - ⁵¹ S. Datta and B. Das, *Appl. Phys. Lett.* **56**, 665 (1990).
 - ⁵² A. Manchon, H. C. Koo, J. Nitta, S. M. Frolov, and R. A. Duine, *Nat. Mater.* **14**, 871 (2015).
 - ⁵³ A. Furusaki, *Phys. B (Amsterdam)* **203**, 214 (1994).
 - ⁵⁴ Y. Asano, *Phys. Rev. B* **63**, 052512 (2001).
 - ⁵⁵ Y. Asano, *Phys. Rev. B* **64**, 224515 (2001).
 - ⁵⁶ P. A. Lee and D. S. Fisher, *Phys. Rev. Lett.* **47**, 882 (1981).
 - ⁵⁷ A. M. Clogston, *Phys. Rev. Lett.* **9**, 266 (1962).
 - ⁵⁸ B. S. Chandrasekhar, *Appl. Phys. Lett.* **1**, 7 (1962).
 - ⁵⁹ N. M. Chitchev, W. Belzig, Y. V. Nazarov, and C. Bruder, *JETP Lett.* **74**, 323 (2001).
 - ⁶⁰ J. Cayssol and G. Montambaux, *J. Magn. Magn. Mater.* **300**, 94 (2006).
 - ⁶¹ A. V. Zaitsev, *Zh. Eksp. Teor. Fiz.* **86**, 1742 (1984) [*JETP* **59**, 1015 (1984)].
 - ⁶² I. O. Kulik, *ZhETF* **49**, 1211 (1966) [*JETP* **22**, 841 (1966)].